Results in Physics 7 (2017) 2718–2727

Contents lists available at ScienceDirect

Results in Physics

journal homepage: www.journals.elsevier.com/results-in-physics

The impact of kaolin dehydroxylation on the porosity and mechanical integrity of kaolin based ceramics using different pore formers

David O. Obada [a,*], David Dodoo-Arhin [b,d,*], Muhammad Dauda [a], Fatai O. Anafi [a], Abdulkarim S. Ahmed [c], Olusegun A. Ajayi [c]

[a] Department of Mechanical Engineering, Ahmadu Bello University, Zaria, Nigeria
[b] Department of Materials Science and Engineering, University of Ghana, Legon, Ghana
[c] Department of Chemical Engineering, Ahmadu Bello University, Zaria, Nigeria
[d] Institute of Applied Science and Technology, University of Ghana, Legon, Ghana

ARTICLE INFO

Article history:
Received 20 April 2017
Received in revised form 19 July 2017
Accepted 20 July 2017
Available online 23 July 2017

Keywords:
Porosity
Kaolin clay
Mechanical property
Lattice defects
Calcination

ABSTRACT

Thermally induced lattice defects in kaolin play a key role in the mechanical integrity of kaolin based ceramics during heat treatment due to their phase transformations. The effects of three types of pore formers (*sawdust, styrofoam and powdery high density polyethylene*) on the porosity and mechanical integrity of kaolin based ceramics have been studied based on their batch formulations. The porosity of the ceramic bodies was experimentally determined, while the structure and chemistry of the materials were elucidated via X-ray diffraction (XRD), scanning electron microscopy (SEM), FTIR, DSC/TG/DTA, and zeta potential. The kaolin-based porous samples sintered at 1150 °C exhibited mullite phase transformation attributed to recrystallization effects. Morphologically, open pores were distributed on the sample surfaces due to larger pathways and available channels of eviction of the pore formers. Compressive strength decreased linearly as apparent porosity increased signifying its correlation. The compressive strength showed to be much more sensitive to defects created by dehydroxylation as micro cracks were observed on the sample with HDPE as pore former which could be as a result of large volume change accompanying phase transformations and sensitivity to the dehydroxylation phase. It is noted that the new pore former (HDPE) used in this study produced ceramic bodies with porosity as high as 67% and hence the least compressive strength.

Introduction

Porous ceramics are gaining increased importance to be used for industrial applications, including separation filters, catalyst supports bioceramics, hot gas filters, desiccants, insulators, acoustic absorbers, sensors, and membrane reactors [1–5]. Usually, these porous ceramics can be made by a conventional powder-processing route also referred to as solid state sintering with the incorporation of some pore-forming agents such as sawdust, starch, graphite, and organic particulates [6], or by injection molding [7], or by gelcasting [8]. Several ways to produce porous bulk ceramics have been reported. One of the most common methods is by burning out the combustible pore formers formulated in the green compacts. The pore-forming *in-situ* technique which exploits the decomposition of starting materials is known to be a good way to prepare porous ceramics with well-distributed pores, and its eco-friendliness is an interesting attribute [4,5,9]. Porosity is usually created by adding a combustible material to the raw material mixture. During firing, the combustible material burns out, and leaves a large fraction of pores within the fired body. Even though starch is the most frequently used pore forming agent possibly due to its biological origin and availability, the difficulties maintaining the pore structure formed by the starch burn out, and the narrow size range of commercially available starch types (typically between 5 and 50 μm) limits its application when large pores are desirable. Polymers emerged as an effective alternative to starch as pore forming agents. They exhibit defect-free burn out at relatively low temperatures. In addition, they are easily mixed with ceramic powder or suspensions [11].

The extensive uses of pore formers are considered to be a major factor for determining morphology in ceramic body fabrication, but the characteristics of pore formers before and during fabrication

* Corresponding authors at: Department of Mechanical Engineering, Ahmadu Bello University, Zaria, Nigeria (D.O Obada) and Department of Materials Science and Engineering, University of Ghana, Legon, Ghana (D. Dodoo-Arhin).
E-mail addresses: obadavid4@gmail.com (D.O. Obada), ddarhin@yahoo.com (D. Dodoo-Arhin).

http://dx.doi.org/10.1016/j.rinp.2017.07.048
2211-3797/

remains unverified. Morphological properties (porosity and pore size) of ceramic bodies depend on the topographies of pore-formers and removal of pore former particle in different sintering steps. Microstructure, porosity and mechanical properties of ceramics can be controlled by quantity, chemical and thermal properties of the pore-former. Also interestingly, the chemical, physical and thermal properties of the base material which in this context is kaolin is of huge significance in understanding the physical and mechanical properties of a ceramic compact. For the development of high-quality ceramic bodies, the following characteristics are of huge significance: particle size distribution (PSD), total porosity ratio, surface quality with the absence of large defects and mechanical properties. Wood, the cheapest lingocellulosic material is the source of the inexpensive wood precursor sawdust [12]. Wood has already been used as a natural composite material which consists of cellulose, hemicellulose and lignin, and forms a cellular microstructure of high porosity, good strength, stiffness and toughness [13]. The advantage of using sawdust over conventional pore formers (e.g. starch) is the achievement of high porous structures economically.

There are numerous kaolin deposits in Nigeria and Ghana, and these deposits differ in a number of ways: *e.g.* the type and amount of impurities, colour, mineralogical content and nature, plasticity, and the fired characteristics [14]. Firing of a green body, which are made of clays with high contents of kaolinite, transforms a green body into a ceramic product [15,16]. The green body showcases significant changes of its elastic properties resulting from dehydration at low temperatures, phase changes during dehydroxylation and high-temperature reactions, in addition to densification during sintering [17,18].

The porous nature of kaolin based ceramics which is usually increased by embedding with pore formers makes them susceptible to failure. This leads to breakage during processing, transportation and usage. There is therefore a need to relate the mechanical properties of the fabricated ceramic bodies to their porosity. This is expected to give the correlation of these properties vis-à-vis the industrial applicability. Svinka et al. [19] studied the production of porous alumina ceramics by the slurry casting method and investigated pore formation by elimination of hydrogen as a result of a chemical reaction of aluminium powder with water. The purpose of their study was to determine various ways of producing high porosity alumina ceramics having high mechanical strength and other properties significant for refractory ceramics. Yakub et al. [10] fabricated porous ceramics with three different porosities by the sintering of redart clay and woodchips (sawdust) with a view to developing a ceramic based water filter. The measured mechanical and physical properties were then incorporated into finite element models for the computation of stress distributions due to hydrostatic pressures exerted on the porous clay ceramics by the water in filter with different geometries and supporting configurations. The implications of the results were discussed for potential scale-up and design of a mechanically robust porous ceramic for water filtration. Novais et al. [11] in their work studied the influence of two polymers namely poly-propylene (PP) and polymethyl methacrylate (PMMA) as pore forming agents. The incorporation of the pore formers and their particle size distribution on the porosity, mechanical resistance and thermal conductivity on the produced ceramics was investigated.

In this paper, clay ceramics with three different pore formers (sawdust, high density polyethylene and styrofoam) were produced by the sintering of clay/pore formers mixture with varying ratios by weight. The characteristics of the pore formers were verified using SEM, PSD and DSC techniques. The porosity and compressive strength were experimentally investigated to correlate the synergistic effects of these properties on the final ceramic products. It is also noteworthy that the use of high density polyethylene as a pore former to the best of our knowledge has not been explored as a porogenic material in castable ceramics.

Experimental

Materials and processing

The clay materials that were used in this study were obtained from Kankara and Kibi Kaolin deposits in Nigeria and Ghana respectively and the geographical location and intrinsic properties of the clay has been succinctly described in our previous study [20]. The sawdust (woodchips) used was obtained from a local sawmill in Ghana. The pore formers comprising sawdust, styrofoam (polystyrene) and high density polyethylene (HDPE) powders were processed into fine particles using an IKA A11 Handheld Analytical Mill.

Materials characterization

Characterization of kaolin clay and pore formers

X-ray Fluorescence mineralogical compositions of the clay specimens were determined on a Panalytical Minipal 4 X-ray fluorescence analyzer equipped with an SD detector of a typical resolution of 145 eV and an Omnium software for analysis. The analytical specimens were milled to achieve particle sizes <75 μm, dried at 100 °C and roasted at 1000 °C to determine their Loss on Ignition (LoI) values. About 1 g of each specimen was mixed with 6 g lithium tetraborate flux (Li_2B_4O) and fused at 1050 °C to obtain a stable fused glass bead.

Particle size distribution analyses of the clay samples were carried out using a low-angle laser light scattering (LALLS) technique on a Horiba Scientific, SZ-100 nanoparticle analyzer equipped with a microprocessor with levels of sensitivity in the 0.3 nm to 8 μm

Table 1
Composition of test Samples by weight (Total weight = 100 g).

Sample code.	Kaolin (g)	Plasticizer (Kibi Kaolin) (g)	Saw dust (g)	Styrofoam	High density polyethylene (HDPE)
0% CS	80	20	–	–	–
5%SD	75	20	5	–	–
10%SD	70	20	10		
15%SD	65	20	15		
20%SD	60	20	20		
5%SYF	75	20	–	5	–
10%SYF	70	20	–	10	–
15%SYF	65	20	–	15	–
20%SYF	60	20	–	20	–
5%HDPE	75	20	–	–	5
10%HDPE	70	20	–	–	10
15%HDPE	65	20	–	–	15
20%HDPE	60	20	–	–	20

Table 2
Chemical compositions of the Kankara and Kibi kaolin.

Component	SiO_2	Al_2O_3	Fe_2O_3	TiO_2	MgO	CaO	Na_2O	K_2O	CuO	LoI*
KNK Fraction (wt%)	51.50	28.20	0.91	0.12	0.47	1.21	0.61	1.80	0.02	15.01
KBB Fraction (wt%)	45.81	39.24	0.95	1.46	ND	0.01	0.02	0.84	0.01	11.09

* LoI = Loss on ignition; KNK = Kankara Kaolin; KBB = Kibi Kaolin; ND = Not detected.

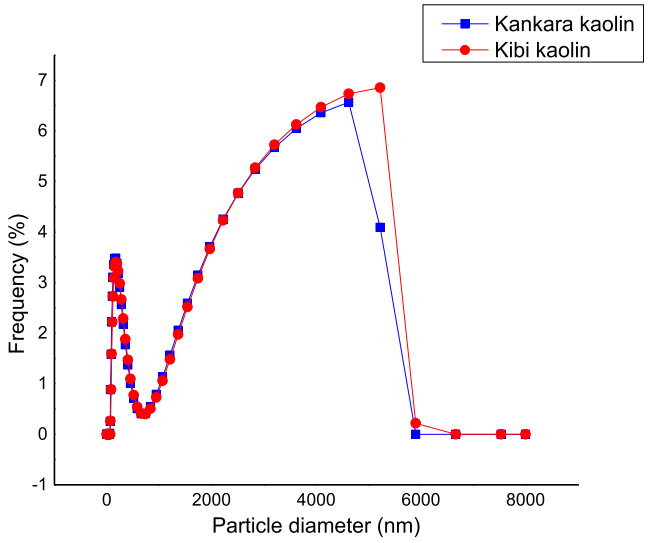

Fig. 1. Particle size distributions of Kankara and Kibi kaolin.

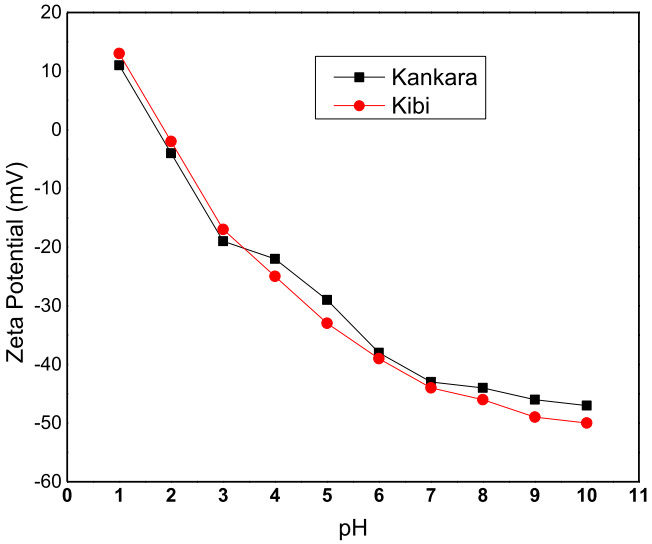

Fig. 2. The zeta potential of the kaolin types in H_2O as a function of pH.

range. In a typical analytical procedure, 10 mg of the clay sample (Kaolin) was added to 10 ml of freshly deionized water and then subjected to continuous ultrasound treatment in an ultrasonic bath for 15mins to ensure dilution and homogenous dispersion before measuring. The electro-kinetic properties of the kaolin clay specimens were determined using a Horiba Scientific, SZ-100-S nanoparticle analyser equipped with Diode pumped frequency doubled laser (532 nm, 10 mW) light source, photomultiplier tubes (PMT) detectors and a microprocessor unit. This unit automatically calculates the electrophoretic mobility of particles and then converts it into the zeta potential. 0.5 g of the kaolin clay sample was ultrasonicated in 100 cm^3 of distilled water for 15 min after which the zeta potential was measured as a function of pH by titration with HCl and NaOH. Each data point is an average of approximately 10 measurements. All measurements were made under ambient temperature conditions.

X-ray powder diffraction (XRD) patterns were collected on a Bruker AXS-D8 Advance Bragg-Brentano diffractometer operating a copper tube (λ = 1.5418 Å) at 40 kV and 30 mA. The XRD patterns of all specimens were recorded in the 10°–90° 2θ range with a step size of 0.017° and a counting time of 14 s per step.

The surface morphology of the samples were carried out on an ultra-high vacuum and high resolution Philips FEI XL-30 FEG scanning electron microscopy equipped with an EVEX EDS and operated at 30 kV and resolution of 2 nm; further images were obtained on a Zeiss (LEO) 1450VP Scanning Electron Microscope (SEM). Samples were metalized with gold/platinum coating prior to the analysis. Images were acquired using a Gatan MiniCL imaging system at various magnifications. The thermal stability of the various phases in the kaolin samples was studied on a NETZSCH, STA 449C Jupiter TG/DTA instrument under air flow of 50 mL/min. Approximately 25 mg of the test specimens were place in an alumina (Al_2O_3) crucible (100 mg capacity), subjected to a linear heating ramp of 100 °C and 700 °C at a rate of 20 °C/min. The test measurements were made for the mass change (loss) of the sample as a function of the temperature and the phase changes by the adsorption or the emission of energy.

To comprehend the thermal transitions of the different pore formers during the sintering process, differential scanning calorimetry (DSC) which measures the changes in heat flow in an analyte due to increase in temperature was carried out on the pore formers. DSC analysis was performed on a Mettler Toledo DSC-2 thermal analyzer in an aluminum crucible from 25 °C to 400 °C at a heating rate of 10 °C/min in nitrogen atmosphere to prevent damage to the particles of the pore formers due to oxidation. Particle size distribution analysis of the pore formers was carried using a low-angle laser light scattering (LALLS) technique on a Horiba Scientific, SZ-100 nanoparticle analyzer. 10 mg of the pore formers plus freshly deionized water (10 mg Pore former +10 mL

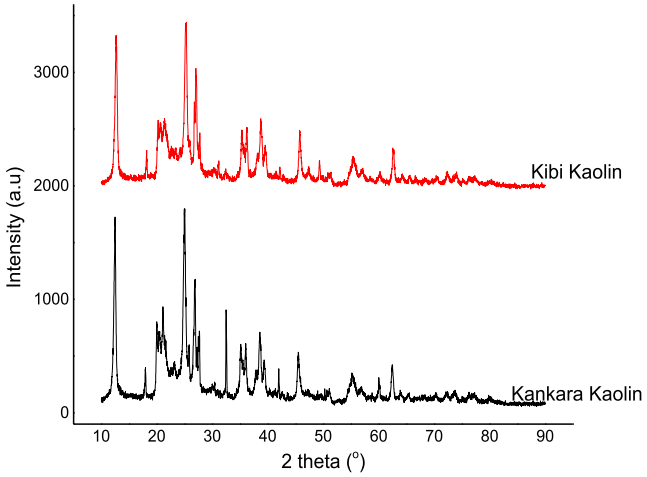

Fig. 3. XRD pattern of Kankara and Kibi Kaolin.

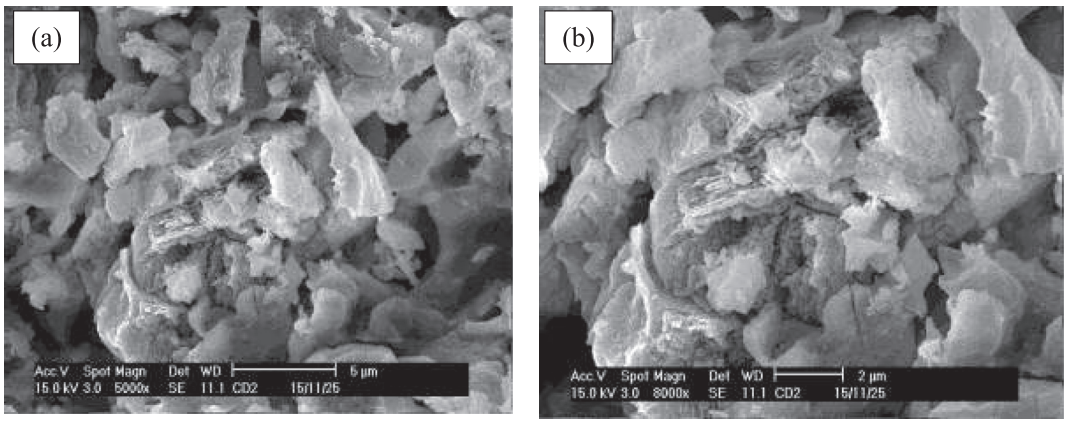

Fig. 4. SEM images of the base Kankara and Kibi kaolin.

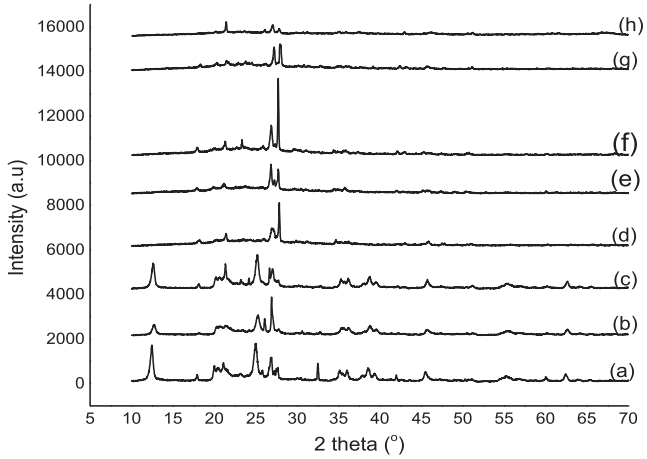

Fig. 5. XRD pattern of Kankara kaolin heated from 30 °C to 900 °C (**a**: 30 °C; **b**: 300 °C; **c**: 400 °C; **d**: 500 °C **e**; 600 °C; **f**: 700 °C; **g**: 800 °C; **h**: 900 °C) the low intensity peaks remaining at 900 °C are indicative of residual quartz.

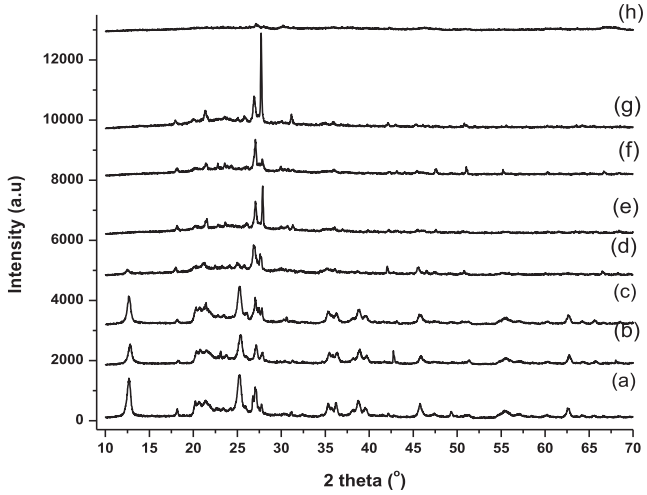

Fig. 6. XRD pattern of Kibi kaolin heated from 30 °C to 900 C (**a**: 30 °C; **b**: 300 °C; **c**: 400 °C; **d**: 500 °C **e**; 600 °C; **f**: 700 °C; **g**: 800 °C; **h**: 900 °C) No peaks remaining at 900 °C.

of water) were subjected to continuous ultrasound treatment in an ultrasonic bath for 15 min to ensure dilution and homogenous dispersion. An FEI Inspect S50 Scanning Electron Microscope operated at 30 kV was employed for the pore formers morphological characterization. Prior to investigation, samples were sputtered with carbon.

Ceramic body fabrication

A quantity of clay was mixed together with measured amounts of the processed (milled) sawdust, styrofoam and powdery high density polyethylene (PHDPE) in four different ratios (clay-to-pore formers) by weight (Table 1). The clay was then blended with the pore formers according to batch formulations using water as the binding agent. The resulting mixtures (clay-pore formers-water) were completely transferred into designed molds and pressed to the same level to ensure compactness and dimensional homogeneity. After about an hour, the as-prepared green body samples were demolded and air dried in the laboratory (temperature of 25 °C, humidity of 43%) for 3 days on boards after which they were further dried at 100 °C in an electric oven for 1 h (to make the green body safer to handle and to remove excess moisture). After drying, the green bodies were subjected to thermal treatment by heating to the sintering temperature of 1150 °C in a muffle furnace. The sintering process was run in two steps; firstly, sintering temperature was setup at 500 °C at a rate of 2 °C/min and held for 2 h so that the pore former would be burned off. Then, the sintering temperature was increased up to 1150 °C at a rate of 5 °C/min and held for 2 h to produce ceramic membranes for the physical and mechanical tests. The samples were heated at 5 °C/min till the desired sintering temperature (1150 °C) was attained. At each sintering temperature, the holding times for different batches were 2 h; after which, the furnace was switched off for cooling and the samples taken after the furnace temperature reached below 100 °C.

Characterization of fabricated ceramic body

The apparent porosities of the samples were measured according to the Archimedes method (using water as immersion fluid) as follows: The fired weights of sintered samples were measured and recorded in air. They were then immersed in a beaker of water. Bubbles were observed as the pores in the specimens were filled with water. Their soaked weights were measured and recorded. This was followed by suspension in a beaker one after the other using a sling and their respective suspended weights measured and recorded. Furthermore, each specimen was lightly wiped with a moistened smooth cotton cloth to remove all excess water from the surface, and the saturated weight, W was recorded. The apparent porosity (the amount of void or pores within a volume of por-

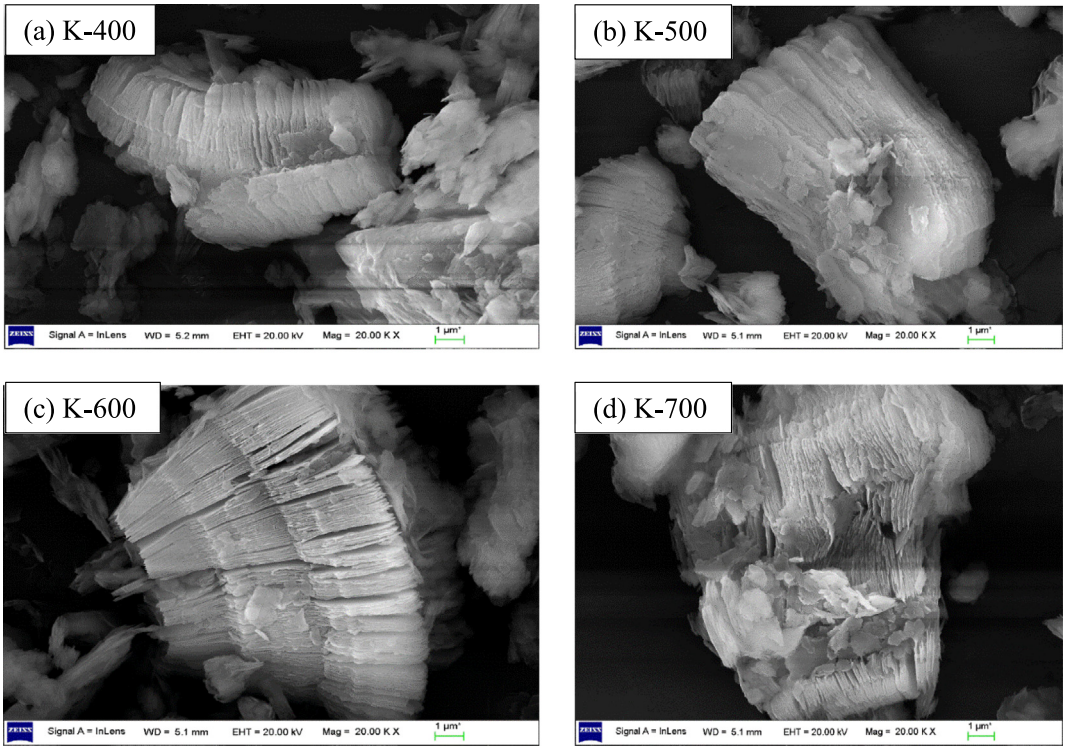

Fig. 7. Scanning electron micrographs of base kaolin heated at (a) 400 °C (b) 500 °C (c) 600 °C (d) 700 °C.

ous solid) of the kaolin based ceramic bodies were calculated using Eq. (1) [21]:

$$\text{Apparent Porosity} = \left(\frac{W - D}{W - S}\right) \times 100 \quad (1)$$

where: D = Weight of fired specimen, S = Weight of fired specimen suspended in water, and W = Weight of soaked specimen suspended in air.

To determine the strength at failure (performance under load) for each sample, compressive strength test was carried out according to ASTM C133-97 (ASTM C133-97, 2003) using a 30-ton Carver hydraulic press testing machine (Carver Press, USA). In total, five specimens were used for the compressive strength measurement and calculated according to Eq. (2):

$$CS = P/BW \quad (2)$$

where P = load at failure and B and W are the respective span and width of the specimens.

Results and discussion

Raw materials characterization

Chemical analysis (XRF), particle size analysis and zeta potential

The chemical analysis data of the Kankara and Kibi kaolin clay types are presented in Table 2. The silica to alumina ratio is found to be 1.81 and 1.16 for the Kankara and Kibi kaolin clay types respectively.

Prior to the usage of the clay samples, the particles size distribution analysis which was conducted as shown in Fig. 1 indicates a broad range of particle sizes (≈1–6000 nm). This range is suitable for close packing configuration applications.

In Fig. 2, the zeta potential of the clay types (Kankara and Kibi) are shown as a function of the pH of dispersant (H_2O). It is known that to obtain dense ceramic components, a number of stages, including mixing, incorporating additives, shape forming, drying and sintering are required. The plot (Fig. 2) show mostly a negative zeta potential in the pH range from 2 to 10. The isoelectric point (the point where the value of the zeta potential is zero) is about pH 2 for the kaolin clay types. Dispersions with a pH near the isoelectric point are unstable. Thus in a pH range of 2, particles are oppositely charged and dispersion flocculates. The interaction is very strong and in this range it is impossible to disperse mixture of kaolin powder and to obtain slurry of good quality without any additives. The variations in zeta potential with pH could be attributed to the nature of the electrical energy field in kaolin [22].

It is well understood that the change in zeta potential in colloid suspensions come from change in surface charge and under acid conditions, kaolinite carried net negative surface charge.

XRD, SEM and phase transformations of Kankara and Kibi clay types

The X-ray diffraction patterns of the two clay types (Kankara and Kibi) is given in Fig. 3. It could be seen from the XRD pattern that the peaks at Bragg's angles of 12.35°, 19.89°, 20.38°, 24.88°, 34.94°, 35.95°, 36.06°, 38.35°, 45.24°, 54.88° and 62.37° responsible for the kaolinite mineral are prominent [23]. The main characteristic peaks of kaolinite (12.35 and 24.88°) for the two patterns are intense.

SEM images of the base kaolin powders used in the fabrication of the ceramic bodies are reported as shown in Fig. 4 at different magnifications. Kaolin powder presents particles with the form of aggregates and have a mixed lamellar or platelet shapes.

Kaolinite ($A1_2O_3{\cdot}2SiO_2{\cdot}2H_2O$), the essential component of kaolin, loses the OH units in its crystal structure at approximately 450 °C, forming an almost amorphous material known as metakaolinite ($Al_2O_3{\cdot}2SiO_2$). Metakaolinite structure is quite unstable, and at about 1000 °C its phase is transformed to γ-alumina, cristobalite (SiO_2) and primary mullite crystals [24–26]. Figs. 5 and 6 shows the ex-situ calcination of Kankara and Kibi kaolin at different temperatures. This is to further buttress the effect of

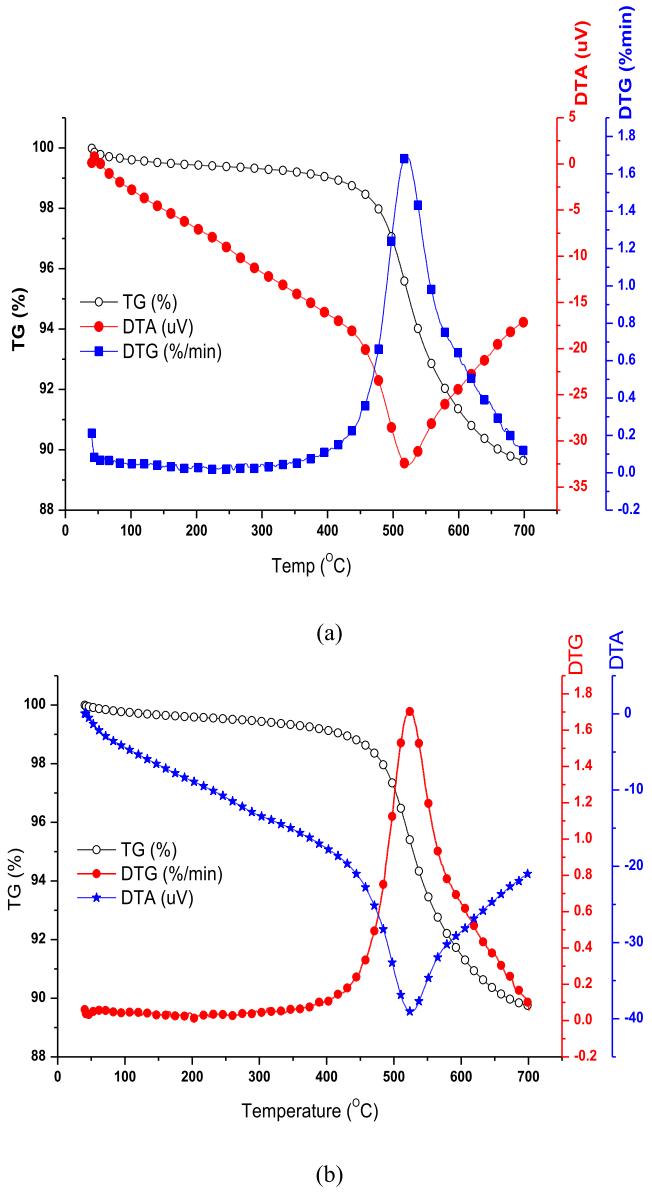

Fig. 8. Thermal analyses (TG, DTG and DTA) of (a) Kankara kaolin and (b) Kibi kaolin.

thermal treatment on the transformation of kaolin. It can be noticed that at 500 °C (d), the peaks responsible for the kaolinite mineral have almost deteriorated completely. This result suggests that some very weakly bound hydroxyl groups of the amorphous phase, as detected by XRD, are released within this temperature range. This is in agreement with other results presented elsewhere [27]. At 900 °C (h), it can be noticed that the low intensity peaks observed for Kankara clay are all of residual quartz remaining in the clays [28]. This is not the case for Kibi kaolin under thermal treatment at that temperature as it shows no residual quartz peak at the calcination temperature which is due to the absence of the quartz phase.

This was followed by SEM of base kaolin (Kankara) heated at the observed dehydroxylation temperature of 400 °C, 500 °C, 600 °C and 700 °C as shown in Fig. 7. The platelet morphology of kaolinite clay reported in the literature and in our previous studies [20,29] which normally portray ordered booklets morphology could be seen as unordered and the booklet morphology deteriorating with increasing calcination temperature.

Dehydroxylation which normally occurs on the phase boundary [24], most times produces a broad endothermic reaction in the 500–600 °C range. Dehydroxylation begins at approximately 450 °C and continues up to around 700 °C [30–32]. The TG curves (Fig. 8) show the weight loss associated with thermal treatment of Kankara and Kibi kaolin up to 700 °C. It can be observed that the remarkable loss occurred between 450 °C and 600 °C and stabilized at about 700 °C for both Kankara and Kibi kaolin. The endotherm as shown in Fig. 8 which corresponds to the dehydroxylation temperature range may be attributed to loss of the hydroxyl units (removal of the chemically bound water) and complete removal of the structure water of the kaolinite structure forming an almost amorphous material which is identified as metakaolin [24,30,33–34]. This result corroborates findings from the ex-situ XRD data in this study. The dehydroxylation temperature of the Kankara and Kibi Kaolin are 526.2 °C and 521.3 °C at enthalpies of −39.07 uV and −32.60 uV respectively.

SEM, PSD and DSC of pore formers

The microstructure of the HDPE (500×) matrix revealed chains of amorphous structure. Ringed and impinged macro-aggregates of crystals are also visible, overall depicting a semi crystalline material. These features indicate that the microstructure of these materials is basically due to HDPE. The microstructure of the styrofoam (500×) shows the typical elliptical shape and large volume of inter-bead voids which are interconnected as indicated by the arrows. Also, the SEM micrograph of saw dust (500×) is presented. It is clear from this image that the surface is rough and highly corrugated. Sawdust is a heterogeneous material consisting of particles of irregular shapes having considerable layers with pores of varying sizes. The finger like morphology typical of raw sawdust is also visible. All these are shown in Fig. 9.

The Particle Size Distribution (PSD) of used pore formers is illustrated in Fig. 10. The Figure shows that there was a wider range of particle sizes for the polymeric pore formers (HDPE and styrofoam) as compared to sawdust.

Fig. 11 depicts the differential scanning calorimetry (DSC) curves of the pore formers. A preliminary look at the plot for styrofoam reveals a glass transition around 70 °C, which did not exhibit a clear melting or freezing temperature in a typical DSC measurement typical of polystyrene. The DSC curve is more stable at high temperatures. The DSC curve for HDPE shows melting and crystallization temperatures respectively. It is noticeable that the polymer started to lose its solid form at around 72 °C which is said to be the glass transition temperature of HDPE and the onset melting point appeared at 186.40 °C which was an endothermic process. It is mentionable that, fully crystalline polymers have no glass transition and their structure remains intact until the melting point. For that reason, a polyethylene commodity (HDPE) is considered as a semi crystalline polymer. As the temperature increases, the rate of heat flow also rises until it reached to the peak point at 194.74 °C which is the melting point of HDPE along with first order transition.

A DSC response from the sawdust of wood biomass shows a peak exotherm at 370.66 °C. As the main components of wood are cellulose, hemicelluloses and lignin, it can be concluded that obtained exotherms refer to the thermal decomposition of mentioned components and inform about interactions occurring between them. This is an evidence that mentioned peak refers to hemicelluloses (similar location), but its shift toward higher temperature evidences that intermolecular forces between hemicelluloses molecules and other molecules exist and are stronger in the case of hemicelluloses present in wood than in the case of hemicelluloses molecules itself (pure hemicelluloses).

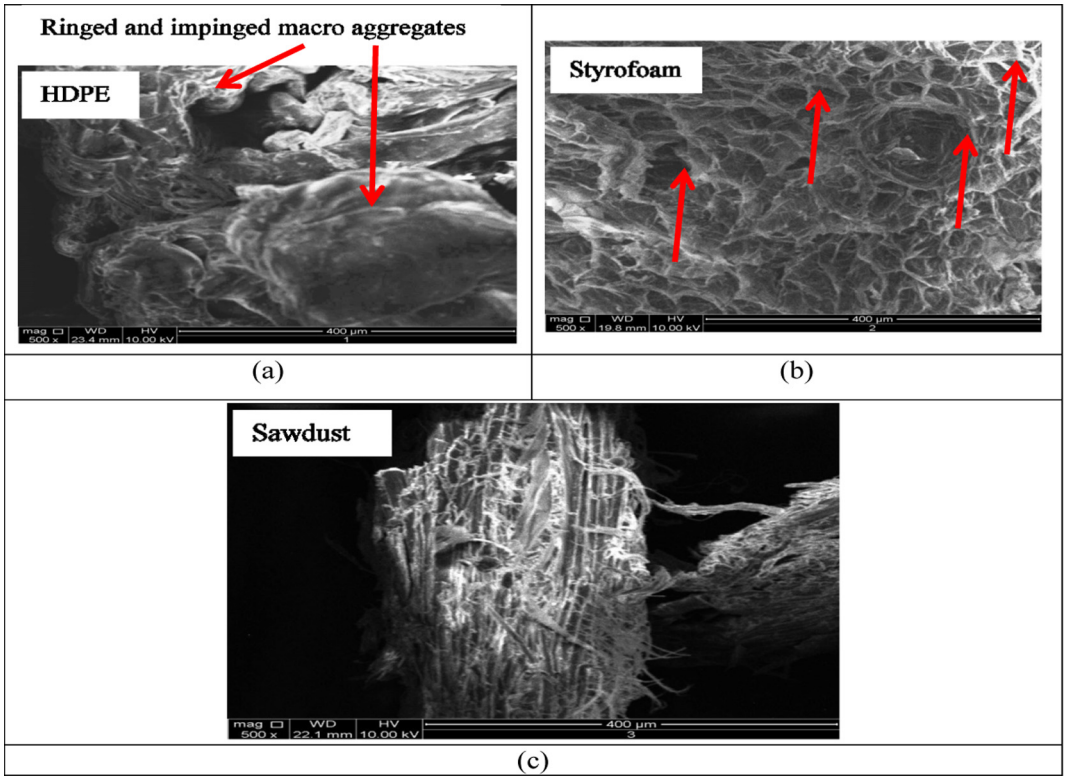

Fig. 9. SEM images of pore formers.

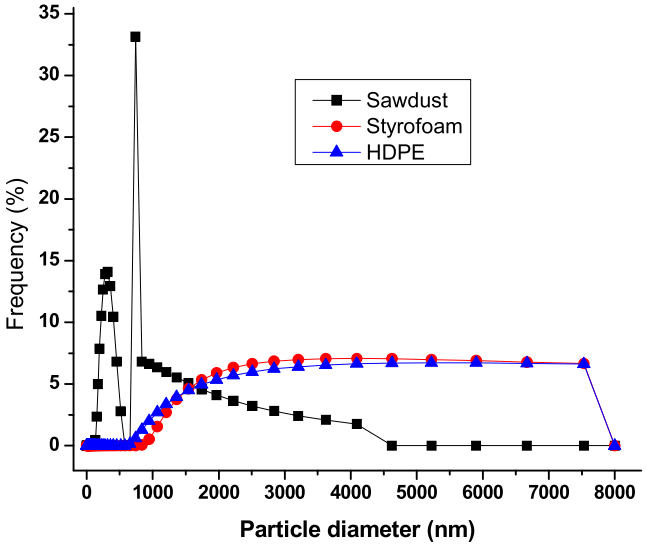

Fig. 10. Particle size distribution for pore formers.

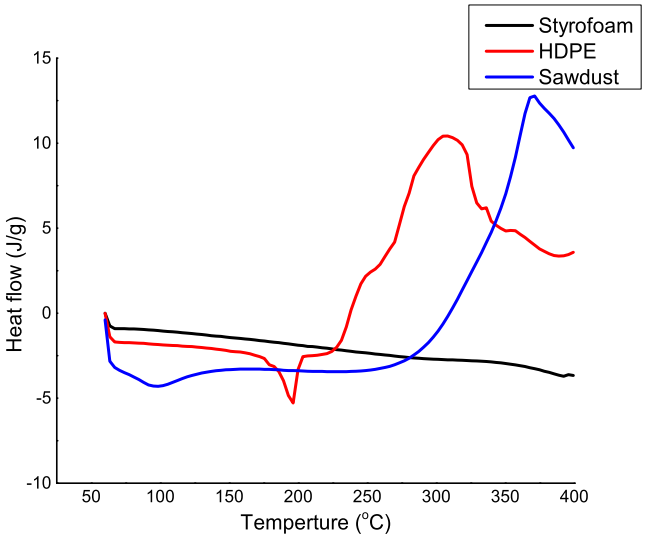

Fig. 11. DSC curves of pore formers.

XRD and SEM of sintered ceramics

In Fig. 12, is depicted a typical XRD spectrum corresponding to ceramic bodies using the different pore formers sintered at 1150 °C for 2 h. The main crystalline phase in the ceramic bodies was found to be mullite. This identified phase is of great importance because of its promising physical and mechanical properties. The results show that the porous ceramics exhibit similar diffraction patterns. This is expected because the pore formers have been burnt out during heat treatment and therefore plays no role in the pattern orientation as presented. The Kankara kaolin clay which is the base material for ceramic fabrication in this study consists predominantly of illite and kaolinite mineral. Approximately above 500 °C, when the kaolinite mineral undergoes an endothermic dehydroxylation process, this transforms it into a disordered alumino-silicate, metakaolinite [25]. The kaolin, which was originally crystalline, is now transformed into metakaolin which is amorphous. This explains the kaolin peaks with less intensity as can be seen from X-ray patterns of the sintered ceramics, and why some of the peaks which is readily observed in kaolin are not obvious. The phases of the porous ceramic samples after thermal treatments shows the transformation phase to mullite which

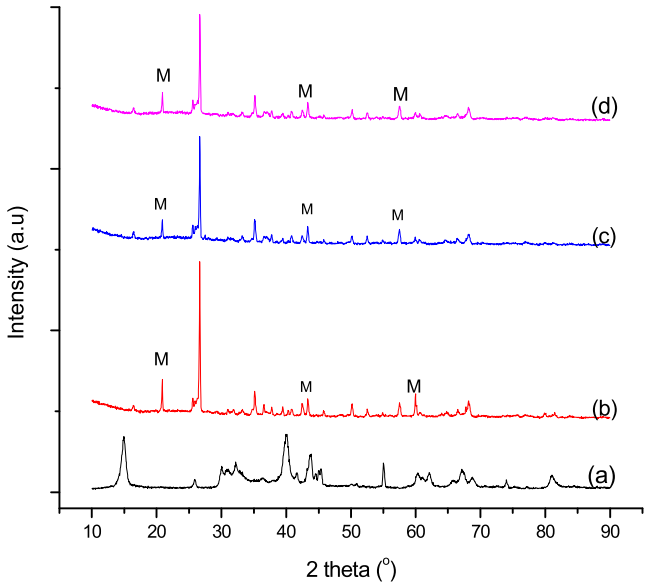

Fig. 12. XRD pattern of: (a) Kankara clay; and sintered porous ceramics with different pore formers- (b) Styrofoam; (c) HDPE; (d) sawdust). M = mullite.

should occur at around the temperature as used in this study (1150 °C).

Fig. 13 shows the SEM images of the porous ceramics and the control sample used in this study. Micrographs of the surface of the sintered ceramics with highest pore former content (20%) are presented in Fig. 13(a)–(c), while the micrograph of the control sample is given in Fig. 13(d). One hypothesis is that the ceramic body with a higher pore former content burns off faster than a ceramic body with a lower pore former content. This is by virtue of larger pathways and available channels of removal of the combustion products (mainly carbon dioxide). As a result, the ceramic body with the higher pore former content has more time to sinter which may be due to the relatively early expulsion of the pore formers.

Correlation of porosity and mechanical strength of samples

The porosities and compressive strengths of the porous samples were evaluated by the expressions described earlier (Eqs. (1) and (2)). Five sets of samples were used for each batch formulation and the average porosities and compressive strengths recorded. Figs. 14 and 15 reveal the variation of percentage inclusion of pore formers to compressive strength and also a composite plot of the variation of compressive strength with porosity. It was important to establish this relationship so as to obtain a realistic correlation for the fabricated bodies based on apparent porosity and compressive strength properties, as these could be said to have a significant effect on the industrial applicability of porous ceramics. The plots show that the strength decreases linearly as apparent porosity increases. The ceramic samples containing HDPE as pore formers by reason of its very high porosity have the least strength. This corroborates the linear correlation obtained. A better fit can be obtained considering a wider range of porosities and similar trends have been observed by other researchers [10,35–37]. The implications of this study are noteworthy. First, the result shows clearly that the mechanical properties of porous ceramics are not a simple function of its density, shrinkage, water absorption among other properties, but depends largely on porosity. Other possible factors that could affect the mechanical strength of porous ceramics include: surface and internal defects (such as cracks) during processing and transportation (mechanical vibration). One way of

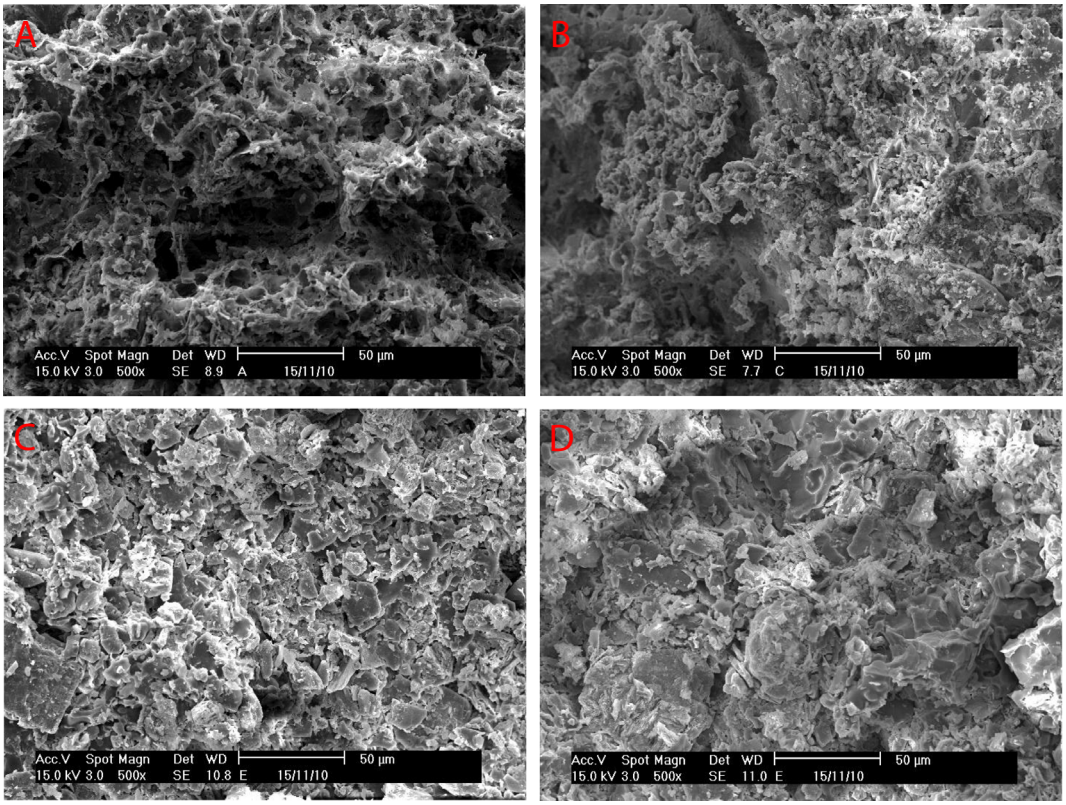

Fig. 13. Scanning electron micrographs of (a) 80:20 sawdust as pore former (b) 80:20 styrofoam as pore former, (c) 80:20 powdery high density polyethylene as pore former (d) 100% kaolin.

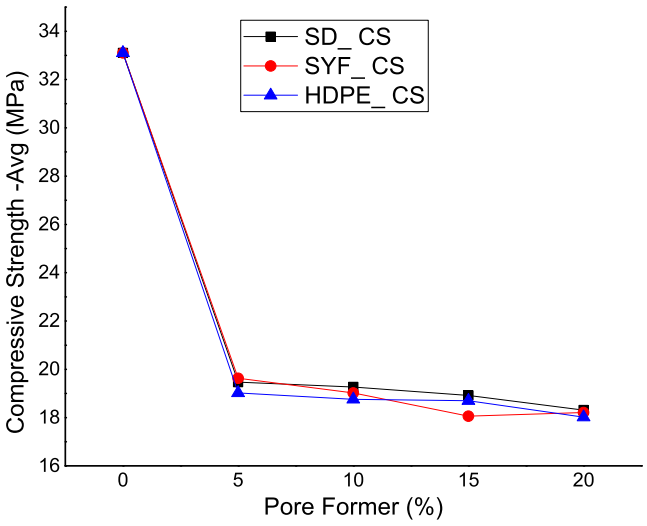

Fig. 14. Variation of percentage pore former content against compressive strength.

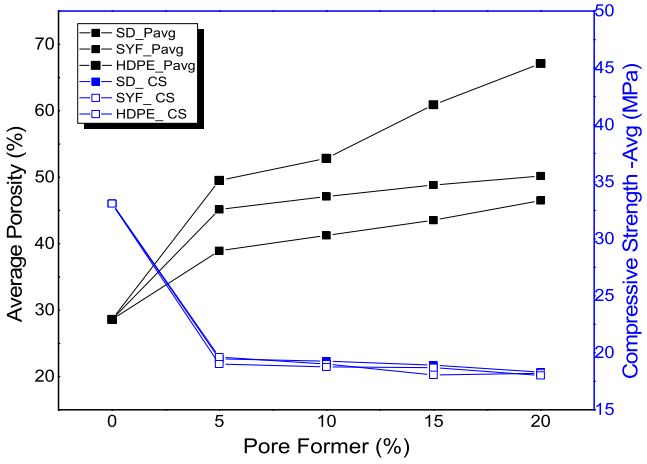

Fig. 15. A composite plot of the variation of percentage pore former content against average values of porosity and compressive strength.

eliminating this hurdle is to fabricate porous ceramics from homogeneous mixtures of clay and pore formers.

The samples after firing exhibited some thermal stability and compactness without indications of severe surface cracks or distortions. This is attributed to the lower melting temperatures of the pore formers. It is commonly believed that the relatively large volume change which accompanies the $\beta \rightarrow \alpha$ transformation of the unsolved quartz grains ($\Delta V/V = -0.68\%$ for free quartz grain) is the basic source of micro-cracking. After removing the weakly bound physically absorbed water, the sample loses the rest of this water and a small amount of the volatile material. The values of the thermal expansion increase up to ~500 °C when dehydroxylation occurs, which leads to a contraction of the sample and dropping of its mass. Following the release of the physically bound water, there is no further change in the structural configuration and composition. The temperature interval of dehydroxylation can be considered a critical stage of the firing process. It is known that an inadequate high rate of heating or cooling leads to cracking of the ceramic body. This was only observed on samples with HDPE as pore former which can also be attributed to the high porosity of the samples. It is noted that the new pore former used in this study produces ceramic bodies with porosity as high as 67%.

Fig. 16. Porous ceramic with HDPE as pore former showing micro cracks.

Fig. 16 shows the micro cracks observed on the sample with HDPE as pore former which could be as a result of large volume change accompanying phase transformations and sensitivity to the dehydroxylation phase.

Mechanical properties like the compressive strength is much more sensitive to defects created by dehydroxylation. An increase of compressive strength during the continuing dehydroxylation (above 450 °C) is a complex phenomenon hence may not be easy to explain. It is known that other constituents (quartz and feldspar) hardly lose their mechanical properties, and metakaolinite, by virtue of its high concentration of crystal defects, must be considered a mechanically weak material [38]. The structure of metakaolinite does not change until ~950 °C, so the effect of the compressive strength increase should be attributed to improving the interface synergy between metakaolinite crystals. Solid phase sintering which has been employed in this study could be a possible relevant mechanism. The cooling stage of the sintered bodies may also be of significance as have been reported elsewhere [39]. The cooling interval can be divided in two parts viz: Above 570 °C, the volume of the quartz grain remains approximately constant, and the glassy cladding tends to contract its volume. The grain is now under the compressive stress and no circumferential cracks can arise. But in the streamlined temperature interval around the $\beta \rightarrow \alpha$ transition of quartz, the quartz grain volume quickly contracts and the circumferential microcracks can then appear around the grains. The microcracks are the outcome of the release of the mechanical stresses caused by the difference in the thermal expansion between the quartz grains and the glass matrix [39–43]. All of these could influence the mechanical properties of porous ceramics.

Conclusions

The porosity of clay ceramics increases with increasing volume fraction of pore formers. The compressive strength decreases with increasing porosity. The mechanical strength of the sintered ceramic body reflects the changes in the structure of the body and the processes therein. These are linked to the escape of the physically bound water, dehydroxylation, the $\alpha \rightarrow \beta$ quartz phase transition, high-temperature reactions and solid-phase sintering during the heating stage of firing. The X-ray diffraction patterns of the kaolin-based porous samples sintered at 1150 °C indicated that they composed of transformed mullite phase which indicates some recrystallization effects. Larger pathways and available channels of eviction of the pore formers led to distributed open surface pore morphologies in the ceramic bodies.

The differential thermal analyses (DTA) and thermogravimetric (TGA) measurements of the kaolin clay types used in this study showed broad endotherms at the dehydroxylation temperature of 526.2 °C and 521.3 °C at enthalpies of −39.07 uV and −32.60 uV respectively. Compressive strength decreases linearly as apparent porosity increases signifying its correlation. It has also been shown that metakaolinization plays a huge role as to the structural integrity of porous ceramics. It is noted that the new pore former used in this study produced ceramic bodies with porosity as high as 67% and hence the least compressive strength.

References

[1] Studart AR, Gonzenbach UT, Tervoort E, et al. Processing routes to macroporous ceramics: a review. J Am Ceram Soc 2006;89(6):1771.
[2] Barea R, Osendi MI, Miranzo P, et al. Fabrication of highly porous mullite materials. J Am Ceram Soc 2005;88(3):777.
[3] Tomita T, Kawasaki S, Okada K. A novel preparation method for foamed silica ceramics by sol-gel reaction and mechanical foaming. J Porous Mater 2004;11 (2):107.
[4] Yan W, Li N, Han BQ. High-strength lightweight spinel refractories. Am Ceram Soc Bull 2005;84(4):9201.
[5] Yan W, Li N. Pore-size distribution and strength of porous mullite ceramics. Am Ceram Soc Bull 2006;85(12):9401.
[6] She JH, Ohji T. Fabrication and characterization of highly porous mullite ceramics. Mater Chem Phys 2003;80(3):610.
[7] Xie Z, Yang J, Huang Y, et al. Study on binder removal process of ceramics injection molding. Bull Chin Ceram Soc 1998;2(2):18.
[8] Liu YF, Liu XQ, Wei H, et al. Porous mullite ceramics from national clay produced by gel casting. Ceram Int 2001;27(1):1.
[9] Deng ZY, Fukasawa T, Ando M, et al. Microstructure and mechanical properties of porous alumina ceramics fabricated by the decomposition of aluminum hydroxide. J Am Ceram Soc 2001;84(11):2638.
[10] Yakub I, Du J, Soboyejo WO. Mechanical properties, modeling and design of porous clay ceramics. Mater Sci Eng A 2012;558:21–9.
[11] Novais RM, Seabra MP, Labrincha JA. Ceramic tiles with controlled porosity and low thermal conductivity by using pore-forming agents. Ceram Int 2014;40(8):11637–48.
[12] Schniewind AP. Concise encyclopedia of wood & wood-based materials. Pergamon Press: MIT Press; 1989.
[13] Bose S, Das C. Preparation and characterization of low cost tubular ceramic support membranes using sawdust as a pore-former. Mater Lett 2013;110:152–5.
[14] Efavi JK, Yaya A, Adeborna S, Fobil J. Development and Comparative Analysis of Aluminosilicate Based Ceramic Filters for Ground Water Defluoridation. Adv Mater Res 2014;936:822–8.
[15] Z. Pospíšil, Z. and A Koller.: Fine Ceramics, Basics of Technology. SNTL/ALFA, Praha 1981 (in Czech).
[16] Pytlík, P. – Sokolář, R.: Building ceramics – technology, properties, applications. Akad. nakladatelství CERM, Brno 2002 (in Czech).
[17] Norton FH. Fine ceramics – technology and application. New York: McGraw-Hill Book Co.; 1970.
[18] Hanykýř V, Kutzendorfer J. Technology of Ceramics. Praha: Silis Praha a Vega Hradec králové; 2000 (in Czech).
[19] R. Svinka, V. Svinka, I Zake., and A Butlers. "Influence of Some Additives on the Properties of Porous Alumina Ceramics", 2009. ISSN 1392-1231.
[20] Obada DO, Dodoo-Arhin D, Dauda M, Anafi FO, Ahmed AS, Ajayi OA. Potentials of fabricating porous ceramic bodies from kaolin for catalytic substrate applications. Appl Clay Sci 2016;132:194–204.
[21] Chesti AR. Refractories: manufacture, properties, and applications. Prentice Hall of India Private Limited: Delhi; 1986.
[22] H. Moayedi, A. Asadi, B.B.K. Huat, and F. Moayedi (2011a). Int. J. Electrochem. Sci.,6(5): 1294-1306.); (R. A. Shrestha, T. D. Pham and M. Sillanpää, Int. J. Electrochem. Sci., 4 (2009) 10, 1387-1394).
[23] N. Salahudeen, Development of Zeolite Y and ZSM-5 composite catalyst from Kankara Kaolin. A Ph.D thesis submitted to the Department of Chemical Engineering, Faculty of Engineering, Ahmadu Bello University, Zaria, Nigeria.2015.
[24] Brindley G, Nakahira M. The kaolinite–mullite reaction series: I., II and III. J Am Ceram Soc 1959;42:311–24.
[25] Bellotto M, Gualtieri A, Artioli G, Clark SM. Kinetic study of the kaolinite-mullite reaction sequence. Part I: kaolinite dehydroxylation. Phys Chem Miner 1995;22(4):207–17.
[26] I. Štubňa, G. Varga and A. Trník, "Investigation of kaolinite dehydroxylations is still interesting", Építôanyag,58, évf. 1, szám, (2006).
[27] Agathopoulos S, Fernandes H, Tulyaganov D, Ferreira J. Preparation of mullite whiskers from kaolinite using $CuSO_4$ as fluxing agent. Mater Sci Forum 2004;455–456:818–21.
[28] Gonzalez Garcıa F, Ruiz Abrio MT, Gonzalez Rodrıguez M. Effects of dry grinding on two kaolins of different degrees of crystallinity. Clay Miner 1991;26(4):549–65.
[29] Obada DO, Dodoo-Arhin D, Dauda M, Anafi FO, Ahmed AS, Ajayi OA, Samotu IA. Physical and mechanical properties of porous kaolin based ceramics at different sintering temperatures. West Indian J Eng 2016;39(1).
[30] Kovo AS, Hernandez O, Holmes SM. Synthesis and characterization of zeolite Y and ZSM-5 from Nigerian Ahoko Kaolin using a novel, lower temperature, metakaolinization technique. J Mater Chem 2009;19(34):6207–12.
[31] Sayin S. Origin of kaolin deposits: Evidence from the Hisarcik (Emet-Kutahya) deposits, Western Turkey. Turkish J Earth Sci 2007;16:77–96.
[32] Dodson V. A study of the reaction between oxygen and mixtures of kaolinite and certain metal chlorides at elevated temperatures. Ohio J Sci 1957;57(1).
[33] I. Štubňa and A. Trnik, "Young's modulus of porcelain mixture after firing in the dehydroxylation region", Ceramics – Silikáty, 51 (2), 102-105, (2007).
[34] Sonuparlak B, Sarikaya M, Aksay I. Spinel Phase Formation during the 980 °C Exothermic Reaction in the Kaolinite-to-Mullite Reaction Series. J Am Ceram Soc 1987;70(11):837–42.
[35] Ward C, French D. *"Analysis and Significance of Mineral Matter in Coal"*, 21st Annual Meeting of the Society for Organic Petrology. Sydney, New South Wales, Australia: The University of New South Wales; 2004.
[36] Knudsen FP. Dependence of mechanical strength of brittle polycrystalline specimens on porosity and grain size. J Am Ceram Soc 1959;42(8):376–87.
[37] Wagh AS, Poeppel RB, Singh JP. Open pore description of mechanical properties of ceramics. J Mater Sci 1991;26(14):3862–8.
[38] Liu DM. Ceram. "Influence of porosity and pore size on the compressive strength of porous hydroxyapatite ceramic". Ceram Int 1997;23(2):135–9.
[39] Kozík T, Štubňa I. Mechanical strength of ceramic material in dehydroxylation region. Silikáty 1981;25:237–41 (in Slovakian).
[40] Freund F. Kaolinite-metakaolinite, a model of a solid with extremely high lattice defect concentration. Ber Deutsche Keram Ges 1967;44:5–13.
[41] Liebermann J. Avoiding quartz in alumina porcelain for high-voltage insulators. Keram Z 2001;53:683–6.
[42] Porte F, Brydson R, Rand B, Riley FL. Creep viscosity of vitreous China. J Am Ceram Soc 2004;87:923–8.
[43] Carty WM, Pinto BM. Effect of filler size on the strength of porcelain bodies. Ceram Eng Sci Proc 2002;23:95–105.